Supporting Information

BRD4 inhibition impairs DNA Mismatch Repair, induces mismatch repair mutation signatures and creates therapeutic vulnerability to immune checkpoint blockade in MMR-proficient tumors

*Yu Fu[#], Bin Yang[#], Yaoyuan Cui[#], Xingyuan Hu, Xi Li, Funian Lu, Tianyu Qin, Li Zhang, Zhe Hu, Ensong Guo, Junpeng Fan, Rourou Xiao, Wenting Li, Xu Qin, Dianxing Hu, Wenju Peng, Jingbo Liu, Beibei Wang, Gordon B. Mills, Gang Chen, and Chaoyang Sun**

Supplementary Figures

Figure S1 BRD4 inhibition down-regulated MMR proteins and impaired MMR function in vitro

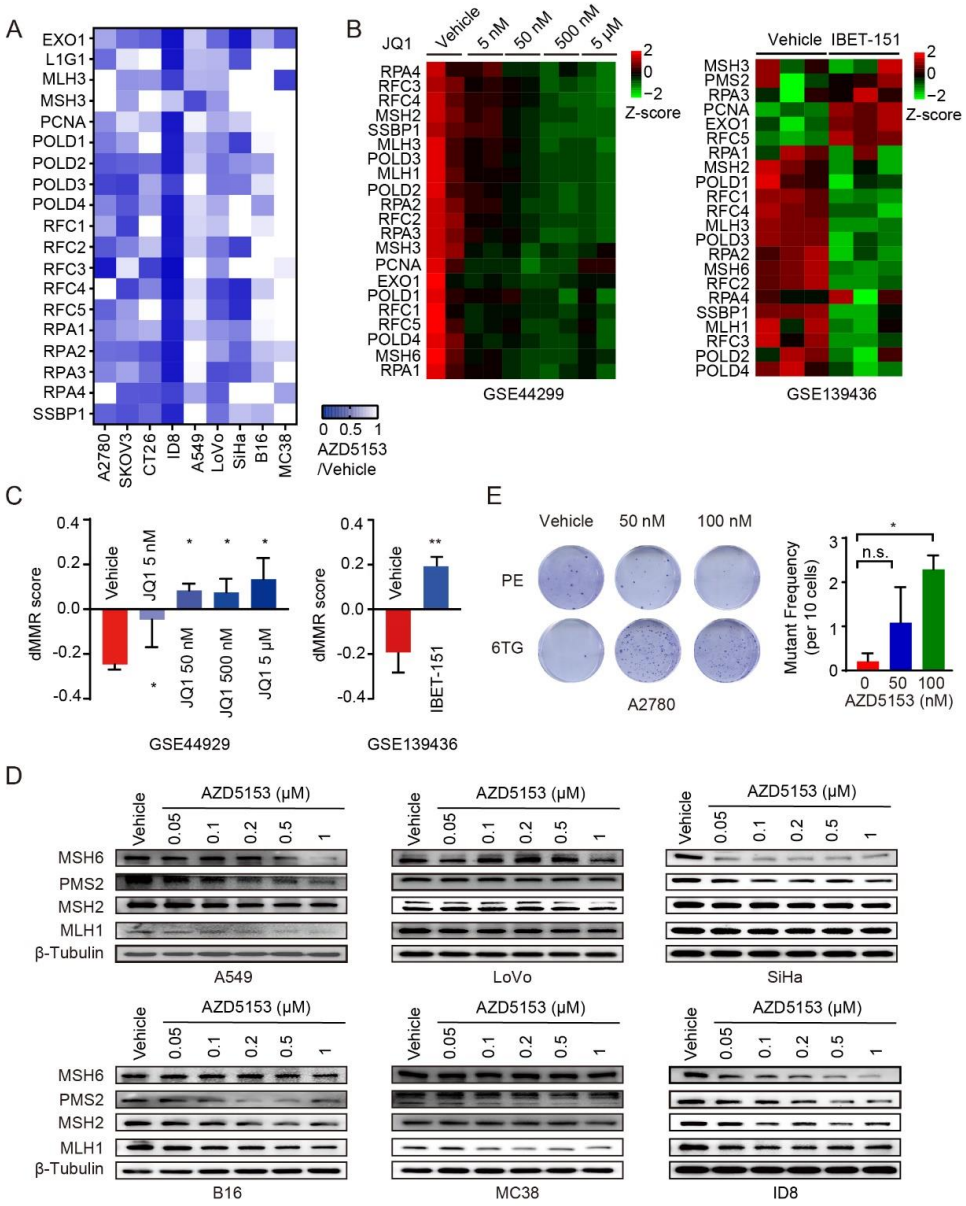

(A) Heatmap showed relative expression changes of 19 MMR system-related genes by RT-qPCR in A2780, SKOV3, CT26, ID8, A549, LoVo, SiHa, B16, and MC38 cell lines treated with 1 μM AZD5153 for 48 hours.

(B) Heatmap shows z-score of the expression of 23 MMR system-related genes based on the GSE44929 (left) and GSE139436 (right) datasets.

(C) dMMR scores for BRD4i-treated cell lines in GSE44929 (left) and GSE139436 (right) datasets. Higher scores represent more defective MMR.

(D) Western blot analysis of MLH1, MSH2, MSH6, and PMS2 proteins in A549, LoVo, SiHa, B16, MC38, and ID8 cell lines treated with the indicated dose of AZD5153 for 72 hours.
(E) Representative pictures (left) and mutant frequency (right) of mutability assay in A2780 treated with vehicle or the indicated dose of AZD5153.

Figure S2 BRD4 transcriptionally regulates MMR genes

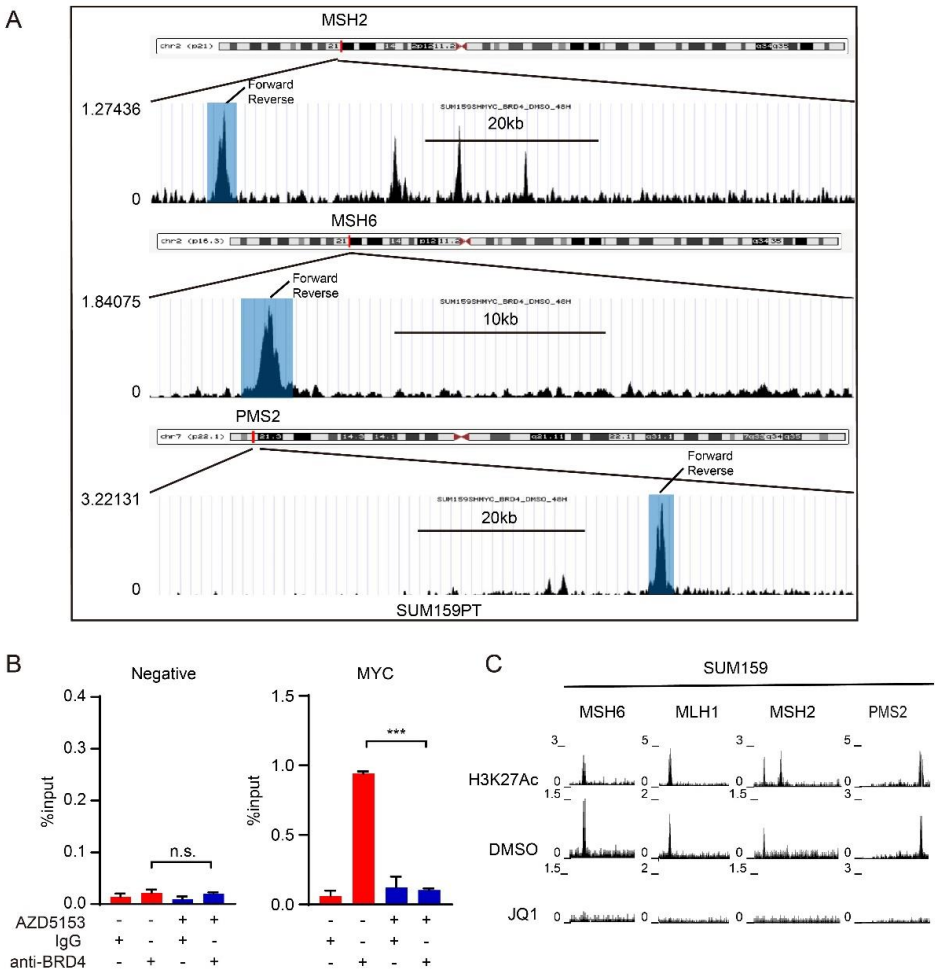

(A) UCSC Genome Browser was used to show BRD4 ChIP-seq signal profiles in the MSH2, MSH6, and PMS2 gene loci. Primers for ChIP-qPCR validation are indicated.

(B) ChIP-qPCR of BRD4 in SKOV3 treated with vehicle or 1 μM AZD5135 for 48 hours. Data represent mean ±SEM from three replicates, two-tailed t tests (*, $p<0.05$; **, $p<0.01$; ***, $p<0.001$)

(C) ChIP sequencing of anti-H3K27ac at the MLH1, MSH2, MSH6, and PMS2 loci in SUM149 cells treated with DMSO or 10 μM JQ1 in GSE131102 dataset.

Figure S3 Prolonged incubation with BRD4i in vitro results in acquisition of dMMR, a dMMR mutational signature that persists despite BRD4i resistance

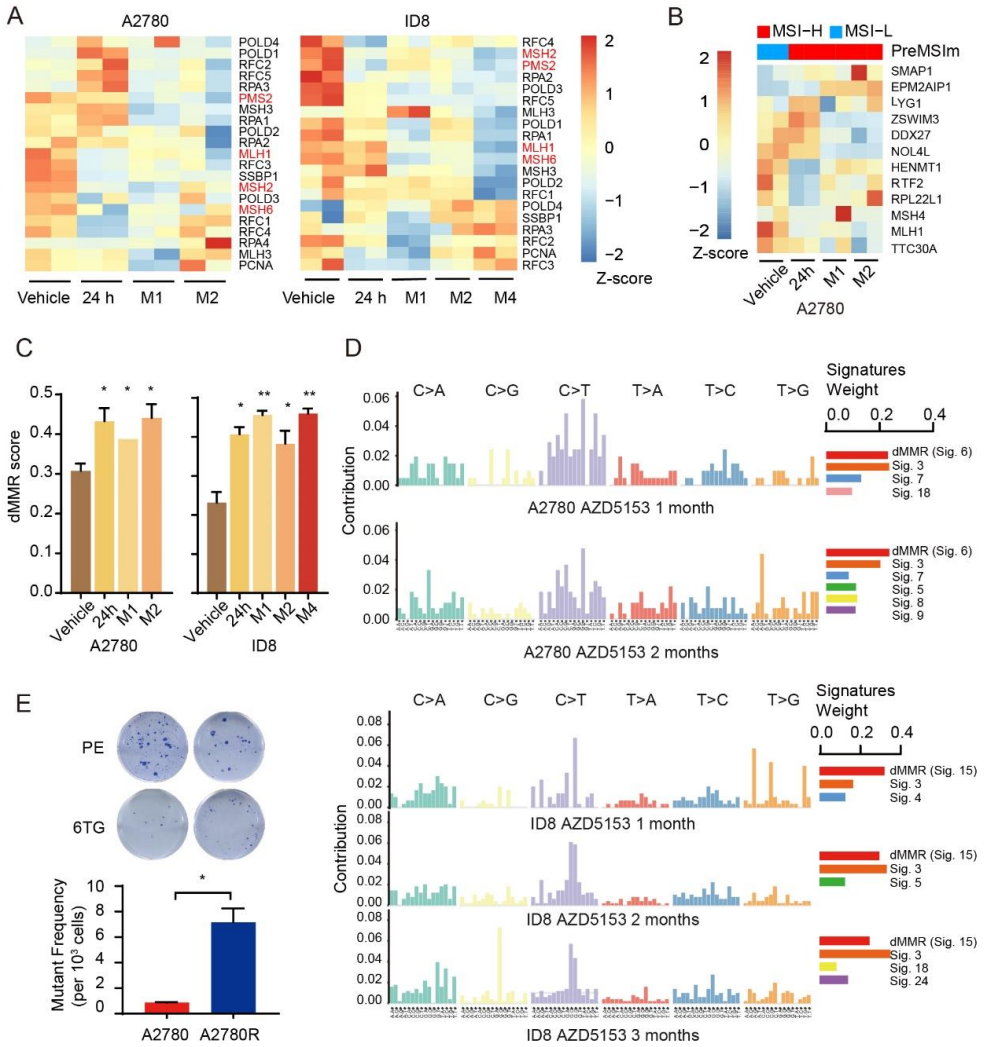

(A) RNA-seq data from A2780 cells treated with vehicle or AZD5153 (24 hours, 1 month, and 2 months) (left) or ID8 cells treated with vehicle or AZD5153 (24 hours, 1 month, 2 months, and 4 months) (right) were analyzed for the expression of 23 MMR related genes. Heatmap shows z-score of relative expression of 23 MMR related genes in indicated treatment.

(B) RNA-seq data from A2780 cells treated with vehicle or AZD5153 (24 hours, 1 month, and 2 months) were analyzed for PreMSIm signature to assess the MSI status. Heatmap shows z-score of relative expression of genes in indicated timepoint of AZD5153 treatment. The top bar indicates the MSI status defined by PreMSIm (blue indicates MSI-low (MSI-L)， representing proficient MMR; red indicates MSI-high (MSI-H), representing dMMR).

(C) RNA-seq data from A2780 cells treated with vehicle or AZD5153 (24 hours, 1 month, and 2 months) (left) and ID8 cells treated with vehicle or AZD5153 (24 hours, 1 month, 2 months, and 4 months)

(right) were analyzed for dMMR scores. Data represent mean ± SD, two-tailed t tests: *, $p<0.05$; **, $p<0.01$; ***, $p<0.001$.

(D) WES data from A2780 cells treated with vehicle or AZD5153 (1 month and 2 months) (upper) and ID8 cells treated with vehicle or AZD5153 (1 month, 2 months, and 4 months) (lower) were analyzed for the mutational signatures and weights of known mutational processes in the Cosmic Signatures for each sample. The proportion of dMMR mutation signatures represented the sum of weights for dMMR-related Cosmic Signatures at each timepoint.

(E) Representative pictures (left) andmutant frequency (right) of mutability assay in parental A2780 cells and A2780R cells. Data are shown as mean ± SEM from each of three independent replicates, two-tailed t tests: *, $p<0.05$; **, $p<0.01$; ***, $p<0.001$.

Figure S4 AZD5153-resistant tumors acquires sensitivity to αPD-L1

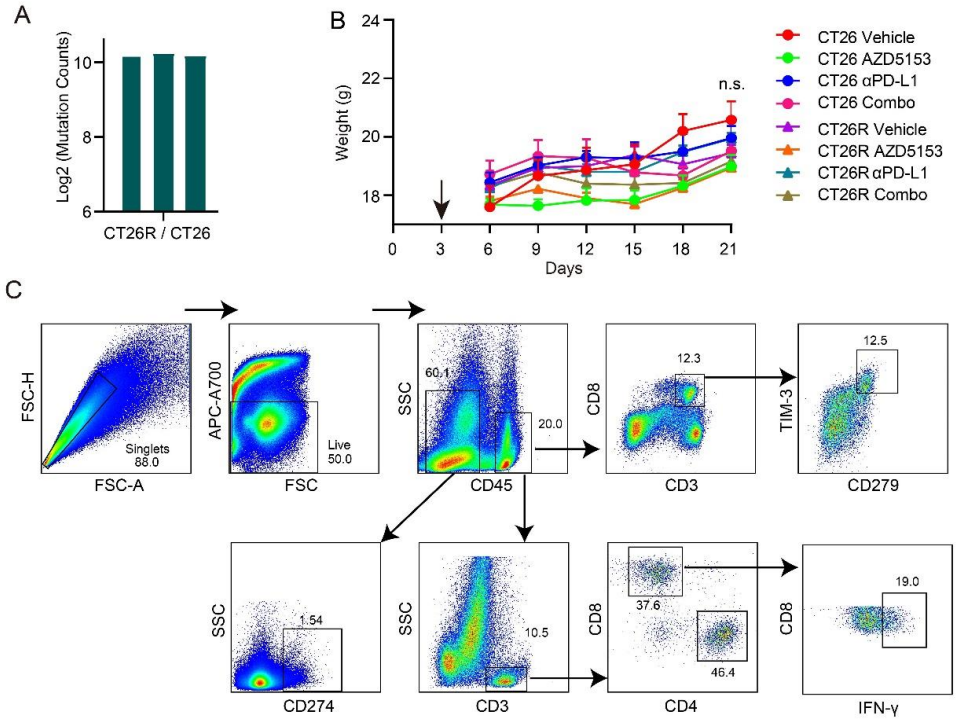

(A) The log2-transformed tumor mutation counts for three replicated CT26R samples, taking CT26 cell line as reference genome and finally assessed by WES sequencing for somatic variants analysis.

(B) Body weight curves after indicated treatment in CT26 and CT26R models. Data represent mean ± SEM. p values were determined by Mann-Whitney test. n.s., not significant.

(C) The gating strategy for effector CD8 T cells and exhausted T cells.

Figure S5 Prolonged exposure to BRD4i in vivo results in acquisition of dMMR, and BRD4i resistance and acquired sensitivity to αPD-L1 therapy

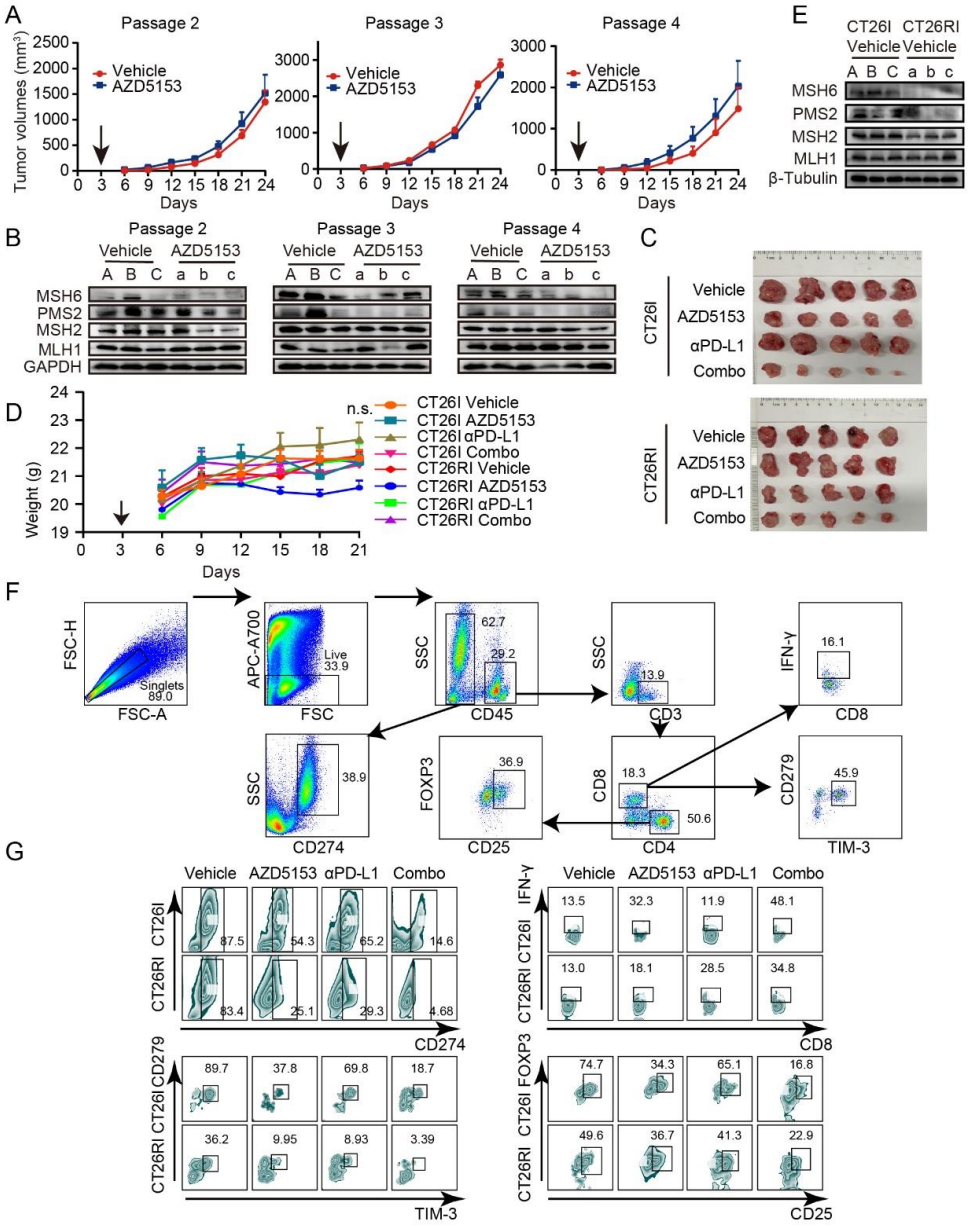

(A) AZD5153-induced resistance in vivo model (CT26RI) mice and the control model (CT26I) (passage 2, 3, and 4) were treated with vehicle (0.5% hydroxypropylmethylcellulose and 0.2% Tween 80), or AZD5153 (1.25 mg/kg per day). Average tumor volumes ± SEM for each cohort was displayed.

(B) Tumor tissues of passage 2, 3, and 4 CT26RI and CT26I models were collected for western blotting of MLH1, MSH2, MSH6, and PMS2.

(C) We transplanted the tumor tissues with same tumor sizes from the fourth generation of CT26I and CT26RI mice into 20 new BALB/c mice respectively. Tumors of CT26I and CT26RI were

further randomized into various treatment groups after implantation: vehicle (0.5% hydroxypropylmethylcellulose and 0.2% Tween 80), AZD5153 (1.25 mg/kg per day, oral gavage), αPD-L1 antibody (200 mg/mouse every 3 days for six times), or a combination of AZD5153 and αPD-L1 antibody. Surgically removed the tumor tissues after treatment complete.

(D) Body weight curves after indicated treatment in CT26I and CT26RI models. Data represent mean ± SEM. p values were determined by Mann-Whitney test. n.s., not significant.

(E) Western blotting of MLH1, MSH2, MSH6, and PMS2 proteins expression in CT26I and CT26RI mice treated with vehicle.

(F) The gating strategy for effector CD8 T cells, exhausted T cells, Treg cells, and PD-L1^{+} tumor cells.

(G) Representative flow cytometry plots of PD-L1^{+} tumor cells (gated on CD45^{-} cells, up left), effector CD8 T cells (CD8^{+} IFN-γ^{+}, gated on CD8^{+} cells, up right), exhausted CD8 T cells (TIM3^{+} PD-1^{+}, gated on CD8^{+} cells, bottom left), and Treg cells (FOXP3^{+} CD25^{+}, gated on CD4^{+} cells, bottom right) in CT26I and CT26RI tumors treated as indicated.

Supplementary Tables

Table S1. The primer sequences for RT-qPCR.

Gene	Forward primer (5′ - 3′)	Reverse primer (5′ - 3′)
Human-EXO1	TGAGGAAGTATAAAGGGCAGGT	AGTTTTTCAGCACAAGCAATAGC
Human-MLH1	CTCTTCATCAACCATCGTCTGG	GCAAATAGGCTGCATACACTGTT
Human-LIG1	GAAGGAGGCATCCAATAGCAG	ACTCTCGGACACCACTCCATT
Human-MLH3	ACAAGCCAAATTGCGTTCTGG	TTCAGCATCAATACTGTTGAGGG
Human-MSH2	AGGCATCCAAGGAGAATGATTG	GGAATCCACATACCCAACTCCAA
Human-MSH3	GTGGACCCCGGATATAAGGTGGG	AAAGGGCAGTCAATTTCCGGG
Human-MSH6	CCAAGGCGAAGAACCTCAAC	ACCAGGGGTAACCCTCCATC
Human-PCNA	CCTGCTGGGATATTAGCTCCA	CAGCGGTAGGTGTCGAAGC
Human-PMS2	CCTATTGATCGGAAGTCAGTCCA	CTACTAACTCCTTTACCGCAGTG
Human-POLD1	ATCCAGAACTTCGACCTTCCG	ACGGCATTGAGCGTGTAGG
Human-POLD2	CCATCAGCCAACAATGCCAC	CTAGCCGGAAGGGTTGTGA
Human-POLD3	GAGTTCGTCACGGACCAAAAC	GCCAGACACCAAGTAGGTAAC
Human-POLD4	ACCCAAGAACCTCAGGACAG	AGTTGAGCCTCTGACACCTC
Human-RFC1	TGGAGAGGCAGTTGCATGAAG	CCTTTCGAGCCTTTTTGGTCT
Human-RFC2	GTGAGCAGGCTAGAGGTCTTT	TGAGTTCCAACATGGCATCTTTG
Human-RFC3	GTGGACAAGTATCGGCCCTG	TGATGGTCCGTACACTAACAGAT
Human-RFC4	CCGCTGACCAAGGATCGAG	AGGGAACGGGTTTGGCTTTC
Human-RFC5	GAAGCAGACGCCATGACTCAG	GACCGAACCGAAACCTCGT
Human-RPA1	GGGGATACAAACATAAAGCCCA	CGATAACGCGGCGGACTATT
Human-RPA2	GCACCTTCTCAAGCCGAAAAG	CCCCACAATAGTGACCTGTGAAA
Human-RPA3	AGCTCAATTCATCGACAAGCC	TCTTCATCAAGGGGTTCCATCA
Human-RPA4	GTGACCAACTGTGTGAGAGAG	TACACGGTACAACGTCCTGAA
Human-SSBP1	TGAGTCCGAAACAACTACCAGT	CCTGATCGCCACATCTCATTAG
Human-β-actin	CAGCCATGTACGTTGCTATCCAGG	AGGTCCAGACGCAGGATGGCATG
Mouse-Exo1	TGGCTGTGGATACCTACTGTT	ATCGGCTTGACCCCATAAGAC
Mouse-Mlh1	GTTTTACTCCATTCGGAAGCAGT	TGTGAGCGGAAGGCTTTATAGAT
Mouse-Lig1	CCAGCTCATAGTCCCCTCTGA	GTCTTGGCACCTCTAGCAGG
Mouse-Mlh3	AAAGATGCTCCTGAAGTGGGG	TCTTCCACGACTACTGGGCTC
Mouse-Msh2	GTGCAGCCTAAGGAGACGC	CTGGGTCTTGAACACCTCGC
Mouse-Msh3	CAGTGTGCGGGATGACAGG	CCAAGGCGCAGATCACAGG
Mouse-Msh6	CACTCGGCGACACCAAGAA	CTCCGTTGAGATCCTTTGCCT
Mouse-Pcna	TTTGAGGCACGCCTGATCC	GGAGACGTGAGACGAGTCCAT
Mouse-Pms2	CGCAGGTTGAAACTTTTGGCT	CCGTGGCAGGTAGATATAGTGA

Mouse-Pold1	TCGCAGTTTGAGGCGAACC	CTGAGCCCACATAGTGGTCA
Mouse-Pold2	GCAGCGTATCAAACTGAAAGGC	ACCTGAAACCTCCCGTCATCT
Mouse-Pold3	AAGATCGTGACTTACAAGTGGC	ACACCAAGTAGGTAACATGCAG
Mouse-Pold4	ATCACTGACTCCTATCCTGTTGT	TACTGCCAGGCCAGGTCAA
Mouse-Rfc1	ATCCTGTCACCTACGTCTCTG	TGGAGGCTGCCTTTTTACATAC
Mouse-Rfc2	CTGCCGTGGGTTGAAAAATACA	CAGAGGATGCTGGTTGTCTTG
Mouse-Rfc3	CAGAGTGCAGCAATACCCTTT	ACAATAGCATTTGCGGTCTCC
Mouse-Rfc4	ATGCAGGCATTTCTGAAAGGC	CCCAAGGAACTGGTTTGACTT
Mouse-Rfc5	CCAGGACATTCTGAGTACCATTC	GGGCCATAGAGAAGTAGGTGT
Mouse-Rpa1	ACATCCGTCCCATTTCTACAGG	CTCCCTCGACCAGGGTGTT
Mouse-Rpa2	GAGTCCGAGCCCAGCATATTG	CCTGTGAAATCTCGACATCTCCA
Mouse-Rpa3	ACCGTGCTCTGTGCATCTTAT	GGAAGCCCTACAGGGAAAAACT
Mouse-Rpa4	TCAACGGCTATTGAGGGCAG	ACTCATCTGGTTCCCTCGGA
Mouse-Ssbp1	TTCAGTTACTTGGACGAGTAGGT	CGCCACATCTCATTTGTTGCTA
Mouse-β-actin	TGCTGTCCCTGTATGCCTCTG	TGATGTCACGCACGATTTCC

Table S2. The primer sequences for ChIP-qPCR.

Gene	Forward primer (5′ - 3′)	Reverse primer (5′ - 3′)
MLH1	CAAATAACGCTGGGTCCACT	GCTTCTCAGGCTCCTCCTCT
MSH2	GCAACCTACCCTTGCATACAC	GCATCCTTAGTAGAGCTCCTTTCT
MSH6	CCAGAGAGGCAGGGCTTT	GAACTGCTGAGCTCCCCTTC
PMS2	TGCGTCCAAAACTGATGTGT	AATGCATTTGAAGCGAGACC
Negative	CGTTTCCAGCGCATATCTTT	TCACCACAGGGCTCACCTAT
MYC	AGGGATCGCGCTGAGTATAA	TGCCTCTCGCTGGAATTACT

Table S3. The numbers of TCGA cases in Figure 2H

Cancer Type	Total Number	BRD4_MUT, MMR_WT	BRD4_WT, MMR_MUT	BRD4_WT, MMR_WT
BLCA	409	11	35	363
BRCA	1024	4	27	993
CESC	289	7	11	271
COAD	401	16	43	342
ESCA	183	3	9	171
GBM	397	5	5	387
HNSC	508	7	16	485

KIRP	281	2	9	270
LUAD	516	4	31	481
LUSC	483	12	26	445
SKCM	456	20	44	392
STAD	435	11	32	392
UCEC	502	10	66	426